

Towards High-performance Spiking Transformers from ANN to SNN Conversion

Zihan Huang
Peking University
Beijing, China
hzh@stu.pku.edu.cn

Xinyu Shi
Peking University
Beijing, China
xyshi@pku.edu.cn

Zecheng Hao
Peking University
Beijing, China
1900012989@pku.edu.cn

Tong Bu
Peking University
Beijing, China
putong30@pku.edu.cn

Jianhao Ding
Peking University
Beijing, China
djh01998@stu.pku.edu.cn

Zhaofei Yu*
Peking University
Beijing, China
yuzf12@pku.edu.cn

Tiejun Huang
Peking University
Beijing, China
tjhuang@pku.edu.cn

Abstract

Spiking neural networks (SNNs) show great potential due to their energy efficiency, fast processing capabilities, and robustness. There are two main approaches to constructing SNNs. Direct training methods require much memory, while conversion methods offer a simpler and more efficient option. However, current conversion methods mainly focus on converting convolutional neural networks (CNNs) to SNNs. Converting Transformers to SNN is challenging because of the presence of non-linear modules. In this paper, we propose an Expectation Compensation Module to preserve the accuracy of the conversion. The core idea is to use information from the previous T time-steps to calculate the expected output at time-step T . We also propose a Multi-Threshold Neuron and the corresponding Parallel Parameter normalization to address the challenge of large time steps needed for high accuracy, aiming to reduce network latency and power consumption. Our experimental results demonstrate that our approach achieves state-of-the-art performance. For example, we achieve a top-1 accuracy of 88.60% with only a 1% loss in accuracy using 4 time steps while consuming only 35% of the original power of the Transformer. To our knowledge, this is the first successful Artificial Neural Network (ANN) to SNN conversion for Spiking Transformers that achieves high accuracy, low latency, and low power consumption on complex datasets. The source codes of the proposed method are available at <https://github.com/h-z-h-cell/Transformer-to-SNN-ECMT>.

*Corresponding author.

Permission to make digital or hard copies of all or part of this work for personal or classroom use is granted without fee provided that copies are not made or distributed for profit or commercial advantage and that copies bear this notice and the full citation on the first page. Copyrights for components of this work owned by others than the author(s) must be honored. Abstracting with credit is permitted. To copy otherwise, or republish, to post on servers or to redistribute to lists, requires prior specific permission and/or a fee. Request permissions from permissions@acm.org.
MM '24, October 28-November 1, 2024, Melbourne, VIC, Australia

© 2024 Copyright held by the owner/author(s). Publication rights licensed to ACM.
ACM ISBN 979-8-4007-0686-8/24/10
<https://doi.org/10.1145/3664647.3680620>

CCS Concepts

• **Computing methodologies** → **Artificial intelligence**.

Keywords

Spiking Neural Networks, Spiking Transformer, ANN-SNN Conversion, Expectation Compensation, Multi-Threshold Neurons

ACM Reference Format:

Zihan Huang, Xinyu Shi, Zecheng Hao, Tong Bu, Jianhao Ding, Zhaofei Yu, and Tiejun Huang. 2024. Towards High-performance Spiking Transformers from ANN to SNN Conversion. In *Proceedings of the 32nd ACM International Conference on Multimedia (MM '24)*, October 28-November 1, 2024, Melbourne, VIC, Australia. ACM, New York, NY, USA, 14 pages. <https://doi.org/10.1145/3664647.3680620>

1 Introduction

Spiking neural networks (SNNs) are a type of neural network model that imitates the mechanisms of biological neurons [1, 18]. They are called the third generation of neural networks [34] due to their biological plausibility and computational efficiency [46, 57]. Neurons in SNNs do not produce output at each time step. Instead, they become active and emit spikes only when their membrane potential reaches a specific threshold. The sparse activity of spikes leads to significantly higher computational efficiency than traditional neural networks [40], especially on neuromorphic chips [6, 7, 35, 37]. However, training large-scale, high-precision, and low-latency SNNs remains challenging due to the non-differentiable nature of spikes.

Currently, there are two main approaches to train SNNs. The first approach is direct training using backpropagation or local learning [13, 15, 28, 36, 52–54, 56, 61, 65]. These methods utilize differentiable continuous functions or spike-time-dependent plasticity strategies to replace the non-differentiable spike emission rules. However, this training process still relies on standard GPUs that are not well-suited for the unique characteristics of SNNs, leading to significant resource consumption and limited performance. The second approach is ANN to SNN conversion [3, 4, 9, 30, 41]. This conversion method does not require any additional training. Instead, it uses pre-trained ANNs and replaces activation functions with

spiking neurons, leveraging the similarity between ReLU activation functions and spike emission rates of integrate-and-fire models. The result SNN model preserves the original ANN's performance but often leads to longer inference times, and the modules that can be successfully converted are limited.

As is well known, Transformers have demonstrated exceptional performance in various vision tasks [5, 12, 24, 33, 38]. Despite numerous efforts to convert CNNs to SNNs, converting Transformer models remains a challenge. This is due to unique nonlinear modules such as layernorm and GELU in Transformers that differ from the ReLU function in CNNs. These modules require interaction between neurons within the same layer and exhibit non-linear characteristics, making it challenging to achieve accurate conversion through the linear piecewise quantization of individual neurons.

This paper proposes a new method to convert Transformers to SNNs. The main challenge lies in handling non-linear modules. To address this, we propose an Expectation Compensation Module (ECM) that calculates expectations and replaces each non-linear module. Specifically, a customized ECM is employed to substitute the matrix product, performing most operations through accumulations. This reduces power consumption and ensures the total output matches the expected result at each time step. To improve the efficiency of minimal spikes, we introduce Multi-Threshold Neurons and the corresponding Parallel Parameter normalization, significantly reducing the required latency and power consumption for inference with comparable accuracy.

Our main contributions are summarized as follows:

- We analyze the challenges of non-linear module conversion in Transformer and introduce a novel solution called the Expectation Compensation Module, which uses the information from the previous time steps to calculate the expected output at the current time step. This module overcomes the limitations of traditional methods with minimal power consumption increase.
- To overcome the issue of slow accuracy improvement over time during Transformer conversion, we propose a Multi-Threshold Neuron and the corresponding Parallel Parameter normalization, substantially reducing power consumption requirements and significantly decreasing latency.
- The proposed method is effective on the ImageNet1k dataset, outperforming existing SNN models in accuracy and significantly reducing power consumption compared to other Transformer models. It achieves a top-1 accuracy of 88.60%, with only a 1% accuracy loss compared to ANN, while reducing energy consumption by 65%.

2 Related Works

ANN-SNN Conversion

The ANN-SNN conversion methods aim to replicate the performance of ANNs by converting pre-trained ANN weights into synaptic weights of SNNs. Cao et al. [4] initially proposed training an ANN with ReLU activation function and then replacing the activation layer with IF neurons. Diehl et al. [10] further narrowed the gap by scaling and normalizing the weights. To address the spike count errors resulting from the hard reset mechanism, soft reset neurons were proposed in Rueckauer et al. [41] and Han et al. [19].

Further research has aimed to minimize conversion errors through various optimization: (1) Optimizing thresholds: Sengupta et al. [43] and Zhang et al. [58] proposed dynamic threshold adjustment strategies during the conversion process. (2) Optimizing membrane potential: Bu et al. [2] demonstrated that setting the initial membrane potential at half the threshold can reduce errors. Hao et al. [21] further suggested analyzing residual membrane potential to eliminate conversion errors. (3) Optimizing the pre-conversion ANN structure: Esser et al. [14] suggested training ANNs with quantized activation values. Ho and Chang [22] introduced a trainable clipping layer (TCL) for threshold determination. Ding et al. [11] proposed a rate norm layer, while others [3, 20, 25, 48] suggested various activation functions to replace ReLU. (4) Optimizing spiking neuronal models. Li et al. [32] introduced a neuron model for burst spikes. Wang et al. [50] proposed a memory-enhanced signed neuron. Li et al. [29] suggested incorporating negative spikes and extending simulation time to improve accuracy with minimal cost.

Previous methods for converting CNNs to SNNs were limited by CNN performance. Jiang et al. [26] introduced Universal Group Operators and a Temporal-Corrective Self-Attention Layer to approximate original Transformers but faced long inference latency and accuracy gaps with the ANN.

In contrast, this paper presents a new method for converting Transformers to SNNs, achieving high accuracy and low latency while reducing network energy consumption.

Directly Trained Transformer in ANNs and SNNs

The Transformer architecture has performed well in the ANN and SNN domains. Initially, Transformers gained prominence in the ANNs with their self-attention mechanisms as proposed by Vaswani et al. [47]. Dosovitskiy et al. [12] then introduced the Vision Transformer (ViT), which divided images into fixed-size patches as token inputs, achieving significant success in computer vision. Fang et al. [16, 17] and Sun et al. [45] further expanded ViT models to one billion parameters, pushing the limits of large-scale visual models.

In the SNN domain, spike-based Transformers quickly emerged, incorporating spike self-attention mechanisms with some floating-point calculations [31, 64]. Subsequently, Zhou et al. [63], Yao et al. [55] and Shi et al. [44] introduced fully event-based Transformers. Wang et al. [51] first trained a modified Transformer and then converted it into a Spiking Transformer. Spike-based Transformers have successfully applied to applications, such as monocular depth estimation [60], single-object tracking with event cameras [59], and automatic speech recognition [49].

In contrast to previous methods that training Transformers from scratch, this paper focuses on converting pre-trained Transformers into SNNs to reduce energy while maintaining performance.

3 Preliminaries

In this section, we first detail the theoretical basis of the conversion process from ANNs to SNNs. Then, we introduce the Vision Transformer (ViT), the ANN architecture we selected for conversion.

3.1 ANN-SNN conversion theory

3.1.1 Neurons in ANNs. In ANNs, for linear or convolution layers in CNNs using the ReLU activation, the output a^l of neurons in

layer l can be formulated as:

$$\mathbf{a}^l = \text{ReLU}(\mathbf{W}^l \mathbf{a}^{l-1}) = \max(\mathbf{W}^l \mathbf{a}^{l-1}, 0), \quad (1)$$

where \mathbf{W}^l represents the weights of the linear transformation or convolution in this layer.

3.1.2 Integrate-and-Fire Neurons in SNNs. For Integrate-and-Fire (IF) neurons in SNNs, let $\mathbf{m}^l(t)$ and $\mathbf{v}^l(t)$ denote the membrane potential of neurons in the l -th layer before and after firing spikes at time-step t , the neural dynamic can be formulated as follows:

$$\mathbf{m}^l(t) = \mathbf{v}^l(t-1) + \mathbf{W}^l \mathbf{x}^{l-1}(t), \quad (2)$$

$$\mathbf{s}^l(t) = H(\mathbf{m}^l(t) - \theta^l), \quad (3)$$

$$\mathbf{x}^l(t) = \theta^l \mathbf{s}^l(t), \quad (4)$$

$$\mathbf{v}^l(t) = \mathbf{m}^l(t) - \mathbf{x}^l(t). \quad (5)$$

where H is the Heaviside step function and θ^l is the neuron threshold in layer l . $\mathbf{s}^l(t)$ is the output spike of layer l . $\mathbf{x}^l(t)$ is the post-synaptic potential and theoretical output of layer l , which equals θ^l if the neuron fires and 0 otherwise. Following [41] and [19], we use the "reset-by-subtraction" mechanism, where $\mathbf{v}^l(t)$ decreases by a value of θ^l if the neuron fires.

3.1.3 ANN-SNN Conversion. Combining Equations (2)-(5), we get

$$\mathbf{v}^l(t) - \mathbf{v}^l(t-1) = \mathbf{W}^l \mathbf{x}^{l-1}(t) - \mathbf{x}^l(t). \quad (6)$$

Summing from time-step 1 to time-step T , we have

$$\frac{\mathbf{v}^l(T) - \mathbf{v}^l(0)}{T} = \frac{\mathbf{W}^l \sum_{i=1}^T \mathbf{x}^{l-1}(i)}{T} - \frac{\sum_{i=1}^T \mathbf{x}^l(i)}{T}. \quad (7)$$

Letting $\Phi^l(T) = \frac{\sum_{i=1}^T \mathbf{x}^l(i)}{T}$, we have

$$\Phi^l(T) = \mathbf{W}^l \Phi^{l-1}(T) - \frac{\mathbf{v}^l(T) - \mathbf{v}^l(0)}{T}. \quad (8)$$

Comparing Equations (1) and (8), $\frac{\mathbf{v}^l(T) - \mathbf{v}^l(0)}{T}$ tends to 0 as T becomes large. This allows $\Phi^l(T)$ in SNNs to approximate \mathbf{a}^l in ANNs.

3.1.4 Parameter normalization. Due to the spike-based communication in SNNs, approximation errors arise since SNN neurons can emit only one spike per time step, limited to a firing rate in the range of $[0, r_{\max}]$, where ANNs do not have such constraints. To prevent approximation errors from excessively low or high firing rates, Diehl et al.[10] and Rueckauer et al.[41] introduced weight normalization to rescale parameters using the following equations:

$$W_{\text{SNN}}^l = W_{\text{ANN}}^l \frac{\lambda^{l-1}}{\lambda^l}. \quad (9)$$

where λ^l is determined by the p -th percentile of the total activity distribution of layer l . Modifying Equation (9) and setting θ_j^l to 1 is equivalent to adjusting the firing threshold on the soft-reset neuron to λ^l [2]. This adjustment ensures that the output $\mathbf{x}^l(t)$ is a spike matrix equal to $\mathbf{s}^l(t)$ and suits the operational dynamics of SNNs.

3.2 Vision Transformer

Vision Transformer (ViT) architecture consists of three core components: Embeddings, Transformer Encoder, and Classification Head.

3.2.1 Embeddings. The process starts by segmenting an image into patches of specific dimensions, viewing them as a sequence of tokens. Each patch undergoes linear embedding with added positional embeddings, enriching the output token vectors with the patch's content and location within the image.

3.2.2 Transformer Encoder. Central to feature extraction, the Transformer Encoder plays a crucial role in various visual tasks. It is divided into two primary segments:

(1) Self-Attention Mechanism. This mechanism calculates a weighted sum of all the values V in a given sequence. The attention weights are determined based on the similarity between a query Q and a key K . The values Q , K , and V are obtained through the input X using weight matrices W^Q , W^K , and W^V respectively. The following equation describes the matrix form of the output calculation for the self-attention mechanism:

$$O = \text{Softmax}\left(\frac{Q^T K}{\sqrt{d}}\right) V = \text{Softmax}\left(\frac{(W^Q X)^T W^K X}{\sqrt{d}}\right) W^V X. \quad (10)$$

where d is the dimension of the key and query vectors.

(2) Feed-Forward Network. Here, the input vector passes through two linear layers and is activated by the GELU function between them.

3.2.3 Classification Head. Features related to the CLS token are directed toward the classification head, which then computes the probabilities for the various classes.

4 Method

In this section, we first analyze the main errors encountered in ANN-SNN conversion. Following this, we propose the Expectation Compensation Module (EC) to preserve the accuracy of non-linear modules. In particular, we detailed a lossless conversion method for the matrix product layer, mainly using additional operations. Additionally, a Multi-Threshold Neuron (MT) is designed to improve the efficiency of minimal spikes, which significantly reduces network latency and energy consumption. The diagram shown in Figure 1 provides an overview of the architecture we utilized.

4.1 Error Analysis of Nonlinear Module in ANN-SNN Conversion

Existing ANN-SNN conversion methods mainly focus on CNNs, which typically employ linear operations, such as linear transformations and convolutions, combined with ReLU activation, as formulated in Equation (1). However, Transformer architecture uses many non-linear operations, such as GELU, softmax, layernorm, and matrix product, which cannot be directly formulated using Equation (1). Consequently, the current conversion theory discussed in Section 3.1 does not apply to Transformers, which can lead to conversion errors.

To be specific, we assume that the outputs of layer $l-1$ in both ANNs and SNNs are identical, denoted as $\mathbf{a}^{l-1} = \Phi^{l-1}(T) = \frac{\sum_{i=1}^T \mathbf{x}^{l-1}(i)}{T}$, and we will compare the outputs \mathbf{a}^l and Φ^l in layer l .

Considering an arbitrary non-linear module in layer l of an ANN, its function can be formulated as:

$$\mathbf{a}^l = F(\mathbf{a}^{l-1}), \quad (11)$$

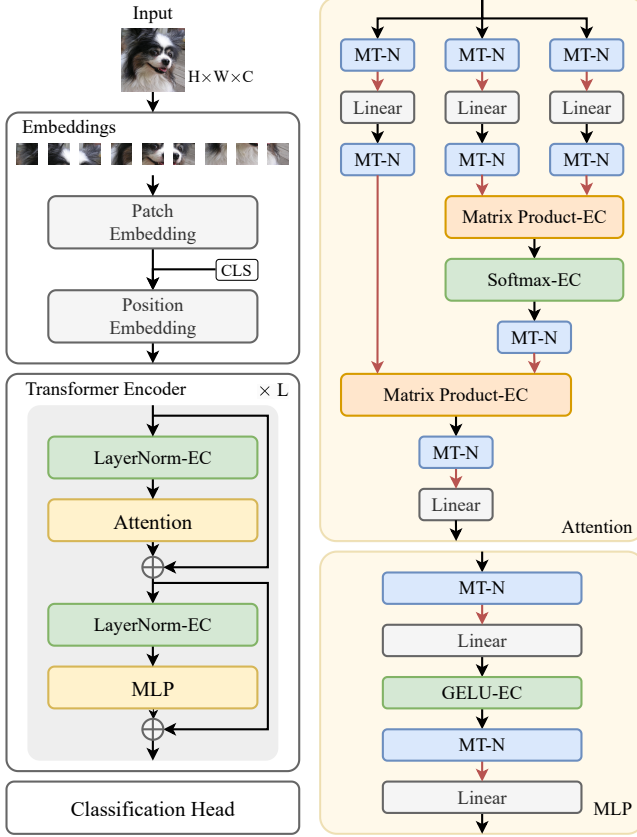


Figure 1: An overview of the proposed architecture, including the whole architecture, Attention, and MLP module.

where F is the function of this layer. Obviously, it cannot be expressed equivalently using Equation (1). In this case, if we do not introduce a further conversion method for this non-linear module, the actual output of the SNN counterpart at time t will be $\mathbf{x}^l(t) = F(\mathbf{x}^{l-1}(t))$. The average output can be formulated as follows:

$$\Phi^l(T) = \frac{\sum_{t=1}^T \mathbf{x}^l(t)}{T} = \frac{\sum_{t=1}^T F(\mathbf{x}^{l-1}(t))}{T}. \quad (12)$$

However, in the case of ANNs, the expected average output can be formulated as:

$$\mathbf{a}^l = F(\mathbf{a}^{l-1}) = F\left(\frac{\sum_{t=1}^T \mathbf{x}^{l-1}(t)}{T}\right). \quad (13)$$

Due to the non-linear nature of the module, we have:

$$\frac{\sum_{t=1}^T F(\mathbf{x}^{l-1}(t))}{T} \neq F\left(\frac{\sum_{t=1}^T \mathbf{x}^{l-1}(t)}{T}\right). \quad (14)$$

This implies that the output $\Phi^l(T)$ of SNNs in Equation (12) is not equivalent to the output \mathbf{a}^l of ANNs in Equation (13), posing challenges for non-linear conversion.

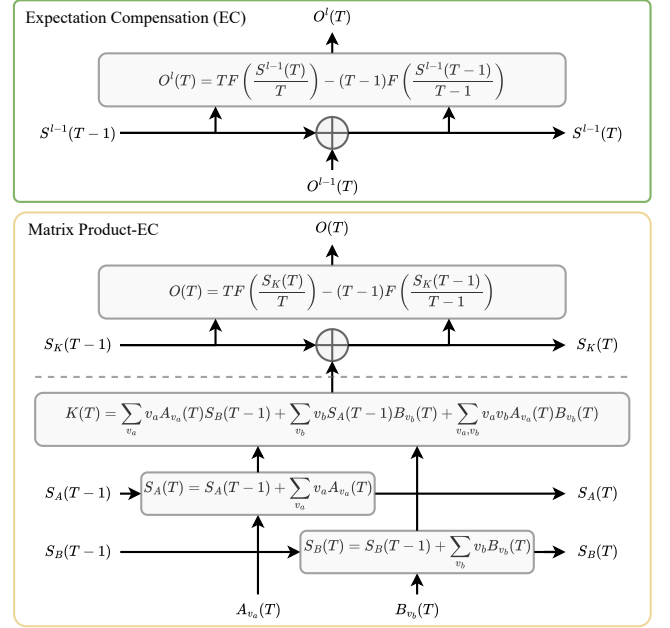


Figure 2: The upper diagram shows the general Expectation Compensation module (EC). The lower diagram shows the Expectation Compensation module for Matrix Product (Matrix Product-EC).

4.2 Expectation Compensation Module

To overcome the challenge of converting non-linear layers, we propose using Expectation Compensation Modules to preserve non-linearity throughout the conversion process by leveraging prior information to compute expectations.

4.2.1 General Expectation Compensation Module.

The theorem below calculates the expected output of the arbitrary non-linear layer at each time step in SNNs.

THEOREM 4.1. Consider a non-linear layer l with a function F . In SNNs, the output of this layer at time t is denoted as $\mathbf{O}^l(t)$. Let $S^l(T)$ be the cumulative sum of layer l outputs up to time T , given by $S^l(T) = \sum_{t=1}^T \mathbf{O}^l(t)$. The expected output of the SNNs at time T is given by:

$$\mathbf{O}^l(T) = TF\left(\frac{S^{l-1}(T)}{T}\right) - (T-1)F\left(\frac{S^{l-1}(T-1)}{T-1}\right). \quad (15)$$

The detailed proof is provided in the supplementary materials. Theorem 7.1 indicates that lossless conversion can be achieved by an accumulator to records $S^{l-1}(T)$ and an optional variable to records $TF(S^{l-1}(T)/T)$ as shown in Figure 2.

4.2.2 Expectation Compensation Module for Matrix Product.

For the matrix product layer, we can convert it into a specialized module that primarily uses additional operations to achieve lossless conversion. The theorem below outlines how to calculate the expected output of the matrix product layer at each time step in SNNs.

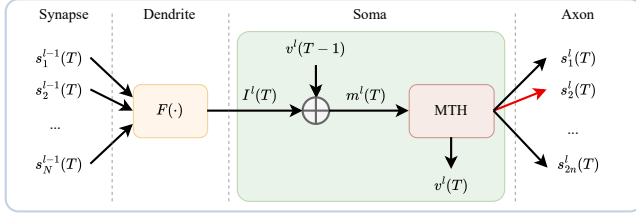


Figure 3: Diagram of MT neuron. MT neuron receives input from nonlinear/linear modules and emits up to one spike.

THEOREM 4.2. Consider a module for matrix product that receives two sets of spike inputs, denoted by $A_{v_a}(t)$ and $B_{v_b}(t)$. These inputs are generated by neurons A and B, respectively, and are characterized by multiple thresholds v_a and v_b , as described in Section 4.3.

We can integrate the input by $A(t) = \sum_{v_a} v_a A_{v_a}(t)$ and $B(t) = \sum_{v_b} v_b B_{v_b}(t)$. Here, $A(t)$ and $B(t)$ are the sum matrices weighted by multiple thresholds v_a and v_b , respectively.

Let $S_A(T) = \sum_{t=1}^T A(t)$ and $S_B(T) = \sum_{t=1}^T B(t)$ represent the cumulative sum of inputs up to time T . We define $S_K(T) = S_A(T)S_B(T)$. Then, the expected output at time T can be formulated as:

$$\mathbf{O}(T) = \frac{1}{T} S_K(T) - \frac{1}{T-1} S_K(T-1), \quad (16)$$

where $S_K(T)$ can be calculated mainly using addition, as described by the following equation:

$$S_K(T) = S_K(T-1) + \mathbf{K}(T) \quad (17)$$

$$\begin{aligned} \mathbf{K}(T) = & \sum_{v_a, v_b} v_a v_b A_{v_a}(T) B_{v_b}(T) + \sum_{v_a} v_a A_{v_a}(T) S_B(T-1) \\ & + \sum_{v_b} v_b S_A(T-1) B_{v_b}(T). \end{aligned} \quad (18)$$

The detailed proof is provided in the supplementary materials. According to Theorem 8.1, the output $\mathbf{O}(T)$ can be obtained through the process illustrated in Figure 2. The main power consumption in this process occurs during the matrix product calculation of $\mathbf{K}(T)$ using spike matrices, which can be implemented through accumulations. Since each position of the input matrix has only one effective threshold at each time, it limits the total number of input spikes, thereby restricting the total number of operations. Combined with the sparsity of spikes, this reduces power consumption at each time step while achieving lossless conversion.

4.3 Multi-Threshold Neuron

4.3.1 Problem of Consumption and Latency.

If we only use the Expectation Compensation Module, neuron communication will remain in a floating-point format. As discussed in Section 5.5, most of the network's power consumption occurs in the linear and matrix product layers. To reduce the network's energy consumption, we introduce spiking neurons before each linear layer and matrix product layer. Thus, we can significantly reduce the network's power consumption by adopting spiking communication.

However, if we only use one threshold, no matter how set, it will result in excessively high firing rates or high inference latency. The

findings in Section 5.4 demonstrate the importance of having large and small thresholds in the Transformer.

4.3.2 The Proposed Solution: Multi-Threshold Neuron.

To tackle the challenges of high power consumption and latency, we propose a Multi-Threshold Neuron (MT neuron).

This neuron model has additional thresholds built upon the base threshold, allowing it to process more information in a single time step. The MT neuron is characterized by parameters including the positive and negative base thresholds, represented as θ_1 and $-\theta_2$, respectively, and the number of thresholds denoted as $2n$. We can refer to λ_p^l as the p -th threshold value of the MT neuron corresponding to index p .

$$\begin{aligned} \lambda_1^l &= \theta_1^l, \lambda_2^l = 2\theta_1^l, \dots, \lambda_n^l = 2^{n-1}\theta_1^l, \\ \lambda_{n+1}^l &= -\theta_2^l, \lambda_{n+2}^l = -2\theta_2^l, \dots, \lambda_{2n}^l = -2^{n-1}\theta_2^l, \end{aligned} \quad (19)$$

As shown in Figure 3, the dynamic of MT neurons is described by:

$$I_j^l(t) = F_j^l(s_1^{l-1}(t), \dots, s_{2n}^{l-1}(t)), \quad (20)$$

$$m_j^l(t) = v_j^l(t-1) + I_j^l(t), \quad (21)$$

$$s_{j,p}^l(t) = MTH_{\theta_1, \theta_2, n}(m_j^l(t)) \quad (22)$$

$$x_j^l(t) = \sum_p s_{j,p}^l(t) \lambda_p^l, \quad (23)$$

$$v_j^l(t) = m_j^l(t) - x_j^l(t). \quad (24)$$

The variables $I_j^l(t), s_j^l(t), x_j^l(t), m_j^l(t)$ and $v_j^l(t)$ respectively represent the input, output, postsynaptic potential, and the membrane potential before and after spikes of the j -th neuron in the l -th layer at time t . Meanwhile, F is a linear or nonlinear function of this layer. The function $MTH_{\theta_1, \theta_2, n}(x)$ can be described using the following piecewise function:

$MTH_{\theta_1, \theta_2, n}(x)$:

$$\left\{ \begin{array}{ll} \lambda_n^l - \frac{\lambda_1^l}{2} \leq x : & s_{j,n}^l(t) = 1, \\ \lambda_{n-1}^l - \frac{\lambda_1^l}{2} \leq x < \lambda_n^l - \frac{\lambda_1^l}{2} : & s_{j,n-1}^l(t) = 1, \\ \dots & \dots \\ \frac{\lambda_1^l}{2} \leq x < \lambda_2^l - \frac{\lambda_1^l}{2} : & s_{j,1}^l(t) = 1, \\ \frac{\lambda_{n+1}^l}{2} \leq x < \frac{\lambda_1^l}{2} : & \text{all the } s_{j,p}^l(t) = 0, \\ \lambda_{n+2}^l - \frac{\lambda_{n+1}^l}{2} \leq x < \frac{\lambda_{n+1}^l}{2} : & s_{j,n+1}^l(t) = 1, \\ \dots & \dots \\ \lambda_{2n}^l - \frac{\lambda_{n+1}^l}{2} \leq x < \lambda_{2n-1}^l - \frac{\lambda_{n+1}^l}{2} : & s_{j,2n-1}^l(t) = 1, \\ x < \lambda_{2n}^l - \frac{\lambda_{n+1}^l}{2} : & s_{j,2n}^l(t) = 1. \end{array} \right. \quad (25)$$

The results of experiments presented in Section 5.4 indicate that although this neuron has multiple thresholds, most of the spikes it generated are concentrated in θ_1 and $-\theta_2$. The spikes generated by other thresholds are minimal, which reduces energy consumption and inference latency.

4.3.3 Parallel Parameter normalization for MT Neuron.

Spike neurons communicate with each other by producing an output spike of either 0 or 1. As for function F in Figure 3.

If F is a Matrix Product-EC function, we only need to send spikes $s^l(t)$ to F as $A_{v_a}(t)$ or $B_{v_b}(t)$.

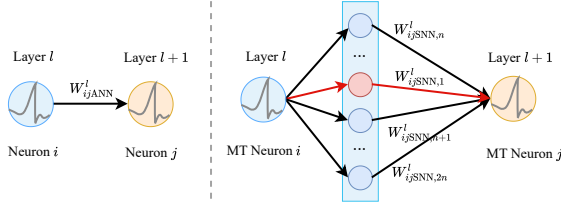


Figure 4: Left: Original connection in ANN. Right: Parallel Parameter normalization of MT neuron in SNN. The MT Neuron extends one connection to $2n$ channels. At each time, only one of the $2n$ channels can emit a spike.

If F is a general nonlinear EC function, we will integrate spike output by $I_j^l(t) = F_j^l(\sum_p s_{i,p}^{l-1}(t)\lambda_p^{l-1})$.

If F is a linear function, $I_j^l(t)$ can be expressed by

$$I_j^l(t) = \sum_i w_{ij}^{ANN} x_i^{l-1}(t) = \sum_i w_{ij}^{ANN} \sum_p s_{i,p}^{l-1}(t)\lambda_p^{l-1} \quad (26)$$

A parallel parameter normalization method is proposed to support spike communication between MT neurons in a linear layer. This method extends the ANN weight to $2n$ weights in the SNN corresponding to $2n$ thresholds of MT neurons, as shown in Figure 4. We update these weights using the following formula:

$$W_{SNN,p}^l = W_{ANN}^l \frac{\lambda_p^{l-1}}{\lambda_1^l} \quad (27)$$

Here, we divide an extra variable λ_1^l to equilibrate parameter size. Let's set $\eta^l = \frac{\theta_2^l}{\theta_1^l}$. This brings the neuron to an equivalent form, which is as follows:

$$I_j^l(t) = \sum_{i,p} w_{ij}^{SNN,p} s_{i,p}^{l-1}(t) \quad (28)$$

$$\theta_{1,new} = 1, \theta_{2,new} = \eta \quad (29)$$

Based on the above discussion, we name this method: Expectation Compensation and Multi-Threshold(ECMT). The overall conversion algorithm can be summarized in Algorithm 1. The conversion is a one-time process, allowing the converted model to be reused without other computations before use.

5 Experimental results

In this section, we first evaluate the proposed method's performance on the ImageNet dataset. Then, we compare our method with state-of-the-art SNN training and ANN-SNN conversion methods. Additionally, we perform ablation experiments on Multi-Threshold Neurons. Finally, we analyze the power consumption of the SNNs converted by our method.

5.1 Experimental Setup

We convert pre-trained Vision Transformer including the ViT-S/16, ViT-B/16, ViT-L/16 with 224 resolution [47], and the EVA model [17] on Imagenet1k dataset [8]. For all Multi-Threshold Neurons, we set n to 8 for ViT-S/16, ViT-B/16, ViT-L/16 and 6 for EVA. And we set threshold percent p to 99. A more detailed setup can be found in supplementary materials.

Algorithm 1 The conversion method using Expectation Compensation Module and Multi-Threshold Neuron(ECMT)

Input: Pre-trained Transformer ANN model $f_{ANN}(W)$; Dataset D ; Time-step T to test dataset; Threshold percent p .

Output: SNN model $f_{SNN}(W, \theta_1, \theta_2, v)$

- 1: **step1:** Obtain the base thresholds θ_1 and θ_2
- 2: **for** length of Dataset D **do**
- 3: Sample minibatch data from D
- 4: Run the data on f_{ANN} and static the activation values before linear and matrix product module at $p\%$ and $(1-p\%)$, setting them as θ_1 and $-\theta_2$ respectively.
- 5: **end for**
- 6: **step2:** Converted to SNN model
- 7: **for** module m in f_{ANN} .Module **do**
- 8: **if** m is Linear Module **then**
- 9: Add a Multi-Threshold Neuron before m
- 10: **else if** m is Matrix Product **then**
- 11: replace m by two Multi-Threshold Neurons followed by a Matrix Product EC Module
- 12: **else if** m is Other Nonlinear Module **then**
- 13: replace m by an EC Module
- 14: **end if**
- 15: **end for**
- 16: Set the base thresholds of MT neurons to corresponding $\theta_1, -\theta_2$ and set the initial membrane potential v to 0.
- 17: $f_{SNN} =$ Parallel Parameter normalization(f_{ANN})
- 18: **return** f_{SNN}

5.2 Experimental results on different model

Based on the provided data, Table 1 compares performance metrics for various architectures. The analysis shows that our SNN approach can achieve comparable accuracies to traditional ANNs with few time steps. Notably, there is only a 1% drop in accuracy observed relative to their ANN counterparts at $T=10$ for ViT-S/16, $T=8$ for ViT-B/16, $T=6$ for ViT-L/16, and as early as $T=4$ for EVA. This trend highlights the efficiency of our conversion strategy, especially within the larger models.

Taking a closer look at the EVA model, our method achieves an impressive 88.60% accuracy at just $T=4$, with a negligible 1% accuracy degradation while using only 35% of the energy required by the equivalent ANN model. These results demonstrate our approach's effectiveness and suggest its potential for significant energy savings without substantially compromising accuracy, particularly in complex and larger-scale model architectures.

5.3 Comparison with the State-of-the-art

Our experiments on the ImageNet1k dataset have pushed the frontiers of neural network efficiency and accuracy. Table 2 provides a compelling narrative of our progress. Our method is unique in that it facilitates the conversion of Transformer models into SNNs, and it stands out for its computational frugality and high accuracy yield. This marks a significant stride over previous state-of-the-art methodologies.

Firstly, our method is designed to be more efficient than direct training approaches. Instead of starting from scratch, we leverage

Table 1: Accuracy and energy consumption ratio of ECMT(Ours) on ImageNet1k dataset

Arch.	Accuracy/Energy	Original (ANN)	Ours (SNN)						
			T=1	T=2	T=4	T=6	T=8	T=10	T=12
ViT-S/16	Acc. (%)	78.04	0.17	10.66	62.85	73.22	76.03	77.07	77.41
	Energy ratio	1	0.06	0.15	0.37	0.59	0.82	1.03	1.25
ViT-B/16	Acc. (%)	80.77	0.24	20.89	69.98	77.81	79.40	80.12	80.38
	Energy ratio	1	0.04	0.12	0.30	0.48	0.66	0.84	1.01
ViT-L/16	Acc. (%)	84.88	3.62	75.38	83.20	84.32	84.60	84.68	84.71
	Energy ratio	1	0.04	0.12	0.27	0.43	0.58	0.74	0.89
EVA	Acc. (%)	89.62	2.49	84.08	88.60	89.23	89.40	89.45	89.51
	Energy ratio	1	0.06	0.15	0.35	0.55	0.74	0.93	1.13

Table 2: Comparison between the proposed method and previous works on ImageNet1k dataset

Method	Type	Arch.	Param. (M)	T	Accuracy (%)
Spikingformer[63]	Direct Training	Spikingformer-4-384-400E	66.34	4	75.85
Spike-driven Transformer[55]	Direct Training	Spiking Transformer-8-768*	66.34	4	77.07
Spikeformer[31]	Direct Training	Spikeformer-7L/3×2×4	38.75	4	78.31
RMP[19]	CNN-to-SNN	VGG-16	138	4096	73.09
SNM[50]	CNN-to-SNN	VGG-16	138	64	71.50
TS[9]	CNN-to-SNN	VGG-16	138	64	70.97
QFFS[29]	CNN-to-SNN	VGG-16	138	4(8)	72.10(74.36)
QCFS[3]	CNN-to-SNN	ResNet-34	21.8	64	72.35
		VGG-16	138	64	72.85
SRP[21]	CNN-to-SNN	ResNet-34	21.8	4(64)	66.71(68.61)
		VGG-16	138	4(64)	66.46(69.43)
MST[51]	Transformer-to-SNN	Swin-T(BN)	28.5	128(512)	77.88(78.51)
STA[26]	Transformer-to-SNN	ViT-B/32	86	32(256)	78.72(82.79)
ECMT(Ours)	Transformer-to-SNN	ViT-S/16	22	8(10)	76.03(77.07)
		ViT-B/16	86	8(10)	79.40(80.12)
		ViT-L/16	307	4(8)	83.20(84.60)
		EVA	1074	4(8)	88.60(89.40)

large pre-trained models to economize on computational efforts and achieve higher accuracy levels than traditional methods. This approach demonstrates our ability to capitalize on the intrinsic efficiencies of pre-trained networks and apply them successfully to SNNs.

Secondly, our technique surpasses the CNN-to-SNN conversion methods in every aspect. Remarkably, even with the ViT-S/16 model at just 8 time steps, we have achieved an accuracy of 76.0%, which outperforms the highest accuracy metrics achieved in previously published CNN-to-SNN works. This highlights the effectiveness of our conversion protocol and confirms its superiority in translating CNN architectures into their spiking counterparts.

Finally, compared to the Swin-T(BN) transformer-to-SNN conversion method mentioned in [51], our approach does not require specific transformer structures for SNN training. Instead, it enables the direct conversion of mainstream ViT models. When compared

to the transformer-to-SNN conversion method in [26], our method can decrease overall energy consumption while requiring extremely lower latency. Based on the above discussion, our process ensures quick turnaround and achieves accuracy within 10 temporal steps.

We conducted experiments using four different models, ViT-S/16, ViT-B/16, ViT-L/16, and EVA, and found that the accuracies achieved at time steps 8, 8, 4, and 4, respectively, were as follows: 76.03%, 79.4%, 83.2%, and 88.6%. The EVA model, in particular, performed exceptionally well at reduced time steps, indicating the robustness of our method and its potential to set new benchmarks in SNN performance.

5.4 The Effect of Multi-Threshold Neuron

To verify the effectiveness of the Multi-Threshold Neuron, we conducted an experiment to explore the model by varying the number of thresholds in the neurons. We denoted the number of thresholds

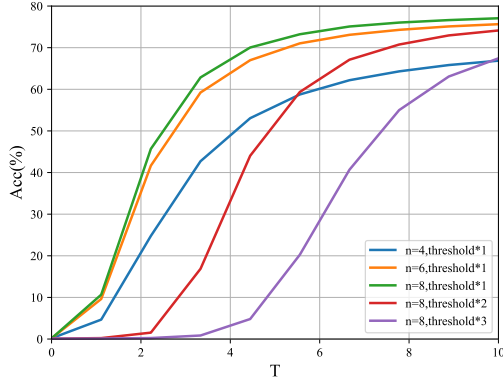


Figure 5: Accuracy under different number and size of thresholds on ViT-S/16, $2n$ denotes the number of thresholds.

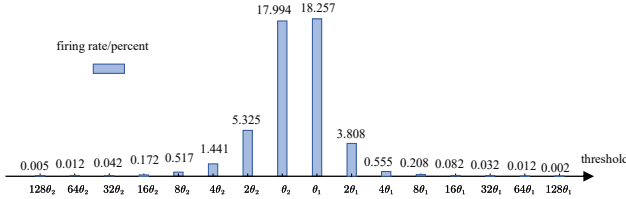


Figure 6: Firing rate at different thresholds

as $2n$ and experimented with $n = 4$, $n = 6$, and $n = 8$. Our results, depicted in Figure 5, illustrate that as the value of n increases, more large thresholds are included. This suggests that having large thresholds is crucial for enhancing performance.

We also increased the base threshold to investigate further while keeping $n = 8$. This allowed us to study the effect of smaller thresholds by their omission. The results were precise: models without small thresholds performed worse than those with both large and small thresholds. Our results showed that both large and small thresholds are crucial for the model. This emphasizes the need for a larger n to achieve low-latency and high-accuracy conversion.

Additionally, we measured the firing rates of spikes associated with each threshold when n was set to 8. The outcomes are presented in Figure 6, which shows that the majority of spikes cluster around the base thresholds, while the spikes generated by other thresholds are minimal. This indicates that adding thresholds consumes less energy but significantly reduces the inference latency.

5.5 Energy Estimation

In order to determine the energy consumption of the SNNs, we begin by calculating the theoretical computational complexity for each module presented in the EVA model, as detailed in Table 3.

We then employ the formula presented in [39] to estimate the energy consumption of SNNs, as detailed in Equation (30):

$$\frac{E_{\text{SNN}}}{E_{\text{ANN}}} = \frac{\text{MACs}_{\text{SNN}} * E_{\text{MAC}} + \text{ACs}_{\text{SNN}} * E_{\text{AC}}}{\text{MACs}_{\text{ANN}} * E_{\text{MAC}}}. \quad (30)$$

Table 3: Theoretical calculation dimensions and actual numerical results of different modules, with image patches $N = 577$, channels $C = 1408$, self-attention heads $N_h = 16$, and MLP hidden layer channels $C_h = 6144$.

Module	Computation	
	Complexity	Results (M)
LayerNorm 1	$N * C$	0.81
Linear qkv	$N * C * 3C$	3431.65
Matrix Product q, k	$Nh * N * (C/Nh)^2$	71.49
Softmax	$Nh * N * N$	5.33
Matrix Product s, v	$Nh * N * N * (C/Nh)$	468.76
Linear out	$N * C * C$	1143.88
LayerNorm 2	$N * C$	0.81
MLP Linear 1	$N * C * Ch$	4991.48
GELU	$N * Ch$	3.54
MLP Linear 2	$N * Ch * C$	4991.48

Here we set $E_{\text{MAC}} = 4.6pJ$ and $E_{\text{AC}} = 0.9pJ$ according to [23].

The original network performs most of its computation in linear and matrix product layers. Our method enables us to implement linear transformations of spikes entirely using accumulations and matrix products primarily using accumulations. As a result, we can estimate the number of multiply operations (MACs_{SNN}) to be zero. We evaluated the total energy consumption ratio of our method compared to the original ANNs, and the results are summarized in Table 1. Our method reaches a high accuracy of 88.60% using only 4 time steps, with a marginal loss of 1% compared to the original ANNs, while consuming only 35% of the energy.

6 Conclusion and Discussion

In this paper, we propose a novel method for converting pretrained Vision Transformers to SNNs with reduced latency. This approach diverges from previous approaches focusing on converting CNNs to SNNs or directly training SNNs, our method converts pre-trained ViTs to SNNs in a low latency. It replaces various modules with a combination of Expectation Compensation Modules and Multi-Threshold Neurons, achieving significantly higher accuracy on the ImageNet dataset with very low latency compared to previous conversion methods. Moreover, the converted models exhibit substantially less energy consumption than the original ANN ViTs. Our method bridges the performance gap between SNNs and ANNs, paving the way for ultra-high-performance SNNs.

Our research has made significant progress in converting Transformers into SNNs with better performance. However, our current method still requires a small amount of multiplication and cannot use accumulations for implementation alone. Although, this issue can be addressed by utilizing hybrid neural networks such as Zhao et al [62], which is based on neuromorphic Tianjic chips [37]. Future work may focus on finding alternative solutions for non-linear modules to eliminate the remaining multiplications. This will make them more suitable for conversion and pave the way for further exploration of the conversion from Transformers to SNNs.

Acknowledgments

This work was supported by the National Natural Science Foundation of China (62176003, 62088102) and the Beijing Nova Program (20230484362).

References

- [1] Sander M Bohte, Joost N Kok, and Johannes A La Poutré. 2000. SpikeProp: Backpropagation for Networks of Spiking Neurons. In *The European Symposium on Artificial Neural Networks*, Vol. 48. 419–424.
- [2] Tong Bu, Jianhao Ding, Zhaofei Yu, and Tiejun Huang. 2022. Optimized Potential Initialization for Low-Latency Spiking Neural Networks. *Proceedings of the AAAI Conference on Artificial Intelligence* 36, 1 (2022), 11–20.
- [3] Tong Bu, Wei Fang, Jianhao Ding, PENGLIN DAI, Zhaofei Yu, and Tiejun Huang. 2022. Optimal ANN-SNN Conversion for High-accuracy and Ultra-low-latency Spiking Neural Networks. In *International Conference on Learning Representations*.
- [4] Yongqiang Cao, Yang Chen, and Deepak Khosla. 2015. Spiking Deep Convolutional Neural Networks for Energy-Efficient Object Recognition. *International Journal of Computer Vision* 113 (2015), 54–66.
- [5] Peng Chen, Yingying ZHANG, Yunyao Cheng, Yang Shu, Yihang Wang, Qingsong Wen, Bin Yang, and Chenjuan Guo. 2024. Multi-scale Transformers with Adaptive Pathways for Time Series Forecasting. In *Proceedings of the International Conference on Learning Representations*.
- [6] Mike Davies, Narayan Srinivasa, Tsung-Han Lin, Gautham Chinya, Yongqiang Cao, Sri Harsha Choday, Georgios Dimou, Prasad Joshi, Nabil Imam, Shweta Jain, Yuyun Liao, Chit-Kwan Lin, Andrew Lines, Ruokun Liu, Deepak Mathaikutty, Steven McCoy, Arnab Paul, Jonathan Tse, Guruguanathan Venkataramanan, Yi-Hsin Weng, Andreas Wild, Yoonseok Yang, and Hong Wang. 2018. Loihi: A Neuromorphic Manycore Processor with On-Chip Learning. *IEEE Micro* 38, 1 (2018), 82–99.
- [7] Michael V. DeBole, Brian Taba, Arnon Amir, Filipp Akopyan, Alexander Andreopoulos, William P. Risk, Jeff Kusnitz, Carlos Ortega Otero, Tapan K. Nayak, Rathinakumar Appuswamy, Peter J. Carlson, Andrew S. Cassidy, Pallab Datta, Steven K. Esser, Guillaume J. Garreau, Kevin L. Holland, Scott Lekuch, Michael Mastro, Jeff McKinstry, Carmelo di Nolfo, Brent Paulovicks, Jun Sawada, Kai Schleppeun, Benjamin G. Shaw, Jennifer L. Klamo, Myron D. Flickner, John V. Arthur, and Dharmendra S. Modha. 2019. TrueNorth: Accelerating From Zero to 64 Million Neurons in 10 Years. *Computer* 52, 5 (2019), 20–29.
- [8] Jia Deng, Wei Dong, Richard Socher, Li-Jia Li, Kai Li, and Li Fei-Fei. 2009. Imagenet: A Large-Scale Hierarchical Image Database. In *IEEE Conference on Computer Vision and Pattern Recognition*. 248–255.
- [9] Shikuang Deng and Shi Gu. 2021. Optimal Conversion of Conventional Artificial Neural Networks to Spiking Neural Networks. In *International Conference on Learning Representations*.
- [10] Peter U. Diehl, Daniel Neil, Jonathan Binas, Matthew Cook, Shih-Chii Liu, and Michael Pfeiffer. 2015. Fast-classifying, High-accuracy Spiking Deep Networks Through Weight and Threshold Balancing. In *Proceedings of International Joint Conference on Neural Networks*. 1–8.
- [11] Jianhao Ding, Zhaofei Yu, Yonghong Tian, and Tiejun Huang. 2021. Optimal ANN-SNN Conversion for Fast and Accurate Inference in Deep Spiking Neural Networks. In *Proceedings of the International Joint Conference on Artificial Intelligence*. 2328–2336.
- [12] Alexey Dosovitskiy, Lucas Beyer, Alexander Kolesnikov, Dirk Weissenborn, Xi-aohua Zhai, Thomas Unterthiner, Mostafa Dehghani, Matthias Minderer, Georg Heigold, Sylvain Gelly, Jakob Uszkoreit, and Neil Houlsby. 2021. An Image is Worth 16x16 Words: Transformers for Image Recognition at Scale. In *International Conference on Learning Representations*.
- [13] Chaoteng Duan, Jianhao Ding, Shiyang Chen, Zhaofei Yu, and Tiejun Huang. 2022. Temporal Effective Batch Normalization in Spiking Neural Networks. *Advances in Neural Information Processing Systems* 35 (2022), 34377–34390.
- [14] Steven K Esser, Jeffrey L. McKinstry, Deepika Bablani, Rathinakumar Appuswamy, and Dharmendra S Modha. 2019. Learned Step Size Quantization. *arXiv preprint arXiv:1902.08153* (2019).
- [15] Wei Fang, Zhaofei Yu, Yanqi Chen, Tiejun Huang, Timothée Masquelier, and Yonghong Tian. 2021. Deep Residual Learning in Spiking Neural Networks. In *Advances in Neural Information Processing Systems*, Vol. 34. 21056–21069.
- [16] Yuxin Fang, Quan Sun, Xinggong Wang, Tiejun Huang, Xinlong Wang, and Yue Cao. 2023. EVA-02: A Visual Representation for Neon Genesis. *arXiv preprint arXiv:2303.11331* (2023).
- [17] Yuxin Fang, Wen Wang, Binhui Xie, Quan Sun, Ledell Wu, Xinggong Wang, Tiejun Huang, Xinlong Wang, and Yue Cao. 2023. EVA: Exploring the Limits of Masked Visual Representation Learning at Scale. In *Proceedings of the IEEE/CVF Conference on Computer Vision and Pattern Recognition*. 19358–19369.
- [18] Wulfram Gerstner, Werner M Kistler, Richard Naud, and Liam Paninski. 2014. *Neuronal Dynamics: From Single Neurons to Networks and Models of Cognition*. Cambridge University Press.
- [19] Bing Han, Gopalakrishnan Srinivasan, and Kaushik Roy. 2020. RMP-SNN: Residual Membrane Potential Neuron for Enabling Deeper High-Accuracy and Low-Latency Spiking Neural Network. In *Proceedings of the IEEE/CVF Conference on Computer Vision and Pattern Recognition*. 13558–13567.
- [20] Jianing Han, Ziming Wang, Jiangrong Shen, and Huajin Tang. 2023. Symmetric-threshold ReLU for Fast and Nearly Lossless ANN-SNN Conversion. *Machine Intelligence Research* 20, 3 (2023), 435–446.
- [21] Zecheng Hao, Tong Bu, Jianhao Ding, Tiejun Huang, and Zhaofei Yu. 2023. Reducing ANN-SNN Conversion Error through Residual Membrane Potential. *Proceedings of the AAAI Conference on Artificial Intelligence* 37, 1 (2023), 11–21.
- [22] Nguyen-Dong Ho and Ik-Joon Chang. 2021. TCL: an ANN-to-SNN Conversion with Trainable Clipping Layers. In *2021 58th ACM/IEEE Design Automation Conference (DAC)*. 793–798.
- [23] Mark Horowitz. 2014. 1.1 Computing’s energy problem (and what we can do about it). In *Proceedings of IEEE International Solid-State Circuits Conference Digest of Technical Papers*. 10–14.
- [24] Jitesh Jain, Jiachen Li, Mang Tik Chiu, Ali Hassani, Nikita Orlov, and Humphrey Shi. 2023. OneFormer: One Transformer To Rule Universal Image Segmentation. In *Proceedings of the IEEE/CVF Conference on Computer Vision and Pattern Recognition*. 2989–2998.
- [25] Haiyan Jiang, Srinivas Anumasa, Giulia De Masi, Huan Xiong, and Bin Gu. 2023. A Unified Optimization Framework of ANN-SNN Conversion: Towards Optimal Mapping from Activation Values to Firing Rates. In *Proceedings of the 40th International Conference on Machine Learning*, Vol. 202. 14945–14974.
- [26] Yizhou Jiang, Kunlin Hu, Tianren Zhang, Haichuan Gao, Yuqian Liu, Ying Fang, and Feng Chen. 2024. Spatio-Temporal Approximation: A Training-Free SNN Conversion for Transformers. In *Proceedings of the International Conference on Learning Representations*.
- [27] A Krizhevsky. 2009. Learning Multiple Layers of Features from Tiny Images. *Master’s thesis, University of Tront* (2009).
- [28] Jun Haeng Lee, Tobi Delbruck, and Michael Pfeiffer. 2016. Training Deep Spiking Neural Networks Using Backpropagation. *Frontiers in Neuroscience* 10 (2016), 228000.
- [29] Chen Li, Lei Ma, and Steve Furber. 2022. Quantization Framework for Fast Spiking Neural Networks. *Frontiers in Neuroscience* 16 (2022), 918793.
- [30] Yuhang Li, Shikuang Deng, Xin Dong, Ruihao Gong, and Shi Gu. 2021. A Free Lunch From ANN: Towards Efficient, Accurate Spiking Neural Networks Calibration. In *Proceedings of the 38th International Conference on Machine Learning*, Vol. 139. 6316–6325.
- [31] Yudong Li, Yunlin Lei, and Xu Yang. 2022. Spikeformer: A Novel Architecture for Training High-Performance Low-Latency Spiking Neural Network. *arXiv preprint arXiv:2211.10686* (2022).
- [32] Yang Li and Yi Zeng. 2022. Efficient and Accurate Conversion of Spiking Neural Network with Burst Spikes. In *Proceedings of the International Joint Conference on Artificial Intelligence*. 2485–2491.
- [33] Xinyu Liu, Houwen Peng, Ningxin Zheng, Yuqing Yang, Han Hu, and Yixuan Yuan. 2023. EfficientViT: Memory Efficient Vision Transformer With Cascaded Group Attention. In *Proceedings of the IEEE/CVF Conference on Computer Vision and Pattern Recognition*. 14420–14430.
- [34] Wolfgang Maass. 1997. Networks of Spiking Neurons: The Third Generation of Neural Network Models. *Neural Networks* 10, 9 (1997), 1659–1671.
- [35] Paul A. Merolla, John V. Arthur, Rodrigo Alvarez-Icaza, Andrew S. Cassidy, Jun Sawada, Filipp Akopyan, Bryan L. Jackson, Nabil Imam, Chen Guo, Yutaka Nakamura, Bernard Brezzo, Ivan Vo, Steven K. Esser, Rathinakumar Appuswamy, Brian Taba, Arnon Amir, Myron D. Flickner, William P. Risk, Rajit Manohar, and Dharmendra S. Modha. 2014. A Million Spiking-neuron Integrated Circuit with a Scalable Communication Network and Interface. *Science* 345, 6197 (2014), 668–673.
- [36] Emre O. Nefeci, Hesham Mostafa, and Friedemann Zenke. 2019. Surrogate Gradient Learning in Spiking Neural Networks: Bringing the Power of Gradient-Based Optimization to Spiking Neural Networks. *IEEE Signal Processing Magazine* 36, 6 (2019), 51–63.
- [37] Jing Pei, Lei Deng, Sen Song, Mingguo Zhao, Youhui Zhang, Shuang Wu, Guanrui Wang, Zhe Zou, Zhenzhi Wu, Wei He, et al. 2019. Towards Artificial General Intelligence with Hybrid Tianjic Chip Architecture. *Nature* 572, 7767 (2019), 106–111.
- [38] Alec Radford, Jong Wook Kim, Chris Hallacy, Aditya Ramesh, Gabriel Goh, Sandhini Agarwal, Girish Sastry, Amanda Askell, Pamela Mishkin, Jack Clark, Gretchen Krueger, and Ilya Sutskever. 2021. Learning Transferable Visual Models From Natural Language Supervision. In *Proceedings of the International Conference on Machine Learning*, Vol. 139. 8748–8763.
- [39] Nitin Rathi and Kaushik Roy. 2020. Diet-snn: Direct Input Encoding with Leakage and Threshold Optimization in Deep Spiking Neural Networks. *arXiv preprint arXiv:2008.03658* (2020).
- [40] Kaushik Roy, Akhilesh Jaiswal, and Priyadarshini Panda. 2019. Towards Spike-based Machine Intelligence with Neuromorphic Computing. *Nature* 575, 7784 (2019), 607–617.
- [41] Bodo Rueckauer, Iulia-Alexandra Lungu, Yuhuang Hu, Michael Pfeiffer, and Shih-Chii Liu. 2017. Conversion of Continuous-Valued Deep Networks to Efficient

- Event-Driven Networks for Image Classification. *Frontiers in Neuroscience* 11 (2017), 294078.
- [42] Olga Russakovsky, Jia Deng, Hao Su, Jonathan Krause, Sanjeev Satheesh, Sean Ma, Zhiheng Huang, Andrej Karpathy, Aditya Khosla, Michael Bernstein, et al. 2015. ImageNet Large Scale Visual Recognition Challenge. *International Journal of Computer Vision* 115 (2015), 211–252.
- [43] Abhronil Sengupta, Yuting Ye, Robert Wang, Chiao Liu, and Kaushik Roy. 2019. Going Deeper in Spiking Neural Networks: VGG and Residual Architectures. *Frontiers in Neuroscience* 13 (2019), 95.
- [44] Xinyu Shi, Zecheng Hao, and Zhaofei Yu. 2024. SpikingResformer: Bridging ResNet and Vision Transformer in Spiking Neural Networks. In *Proceedings of the IEEE/CVF Conference on Computer Vision and Pattern Recognition (CVPR)*. 5610–5619.
- [45] Quan Sun, Yuxin Fang, Ledell Wu, Xinlong Wang, and Yue Cao. 2023. EVA-CLIP: Improved Training Techniques for Clip at Scale. *arXiv preprint arXiv:2303.15389* (2023).
- [46] Amirhossein Tavanaei, Masoud Ghodrati, Saeed Reza Kheradpisheh, Timothée Masquelier, and Anthony Maida. 2019. Deep Learning in Spiking Neural Networks. *Neural Networks* 111 (2019), 47–63.
- [47] Ashish Vaswani, Noam Shazeer, Niki Parmar, Jakob Uszkoreit, Llion Jones, Aidan N Gomez, Ł ukasz Kaiser, and Illia Polosukhin. 2017. Attention is All you Need. In *Advances in Neural Information Processing Systems*, Vol. 30.
- [48] Bingsen Wang, Jian Cao, Jue Chen, Shuo Feng, and Yuan Wang. 2023. A New ANN-SNN Conversion Method with High Accuracy, Low Latency and Good Robustness. In *Proceedings of the International Joint Conference on Artificial Intelligence*. 3067–3075.
- [49] Qingyu Wang, Tielin Zhang, Minglun Han, Yi Wang, Duzhen Zhang, and Bo Xu. 2023. Complex Dynamic Neurons Improved Spiking Transformer Network for Efficient Automatic Speech Recognition. In *Proceedings of the AAAI Conference on Artificial Intelligence*, Vol. 37. 102–109.
- [50] Yuchen Wang, Malu Zhang, Yi Chen, and Hong Qu. 2022. Signed Neuron with Memory: Towards Simple, Accurate and High-Efficient ANN-SNN Conversion. In *Proceedings of the International Joint Conference on Artificial Intelligence*. 2501–2508.
- [51] Ziqing Wang, Yuetong Fang, Jiahang Cao, Qiang Zhang, Zhongrui Wang, and Renjing Xu. 2023. Masked Spiking Transformer. In *Proceedings of the IEEE/CVF International Conference on Computer Vision*. 1761–1771.
- [52] Yujie Wu, Lei Deng, Guoqi Li, Jun Zhu, and Luping Shi. 2018. Spatio-Temporal Backpropagation for Training High-Performance Spiking Neural Networks. *Frontiers in Neuroscience* 12 (2018), 323875.
- [53] Yujie Wu, Rong Zhao, Jun Zhu, Feng Chen, Mingkun Xu, Guoqi Li, Sen Song, Lei Deng, Guanrui Wang, Hao Zheng, et al. 2022. Brain-inspired Global-local Learning Incorporated with Neuromorphic Computing. *Nature Communications* 13, 1 (2022), 65.
- [54] Mingkun Xu, Faqiang Liu, Yifan Hu, Hongyi Li, Yuanyuan Wei, Shuai Zhong, Jing Pei, and Lei Deng. 2024. Adaptive Synaptic Scaling in Spiking Networks for Continual Learning and Enhanced Robustness. *IEEE Transactions on Neural Networks and Learning Systems* (2024), 1–15.
- [55] Man Yao, JiaKui Hu, Zhaokun Zhou, Li Yuan, Yonghong Tian, Bo Xu, and Guoqi Li. 2023. Spike-driven Transformer. In *Advances in Neural Information Processing Systems*, Vol. 36. 64043–64058.
- [56] Huifeng Yin, Hanle Zheng, Jiayi Mao, Siyuan Ding, Xing Liu, Mingkun Xu, Yifan Hu, Jing Pei, and Lei Deng. 2024. Understanding the Functional Roles of Modelling Components in Spiking Neural Networks. *arXiv preprint arXiv:2403.16674* (2024).
- [57] Friedemann Zenke, Sander M. Bohtë, Claudia Clopath, Iulia M. Comşa, Julian Göltz, Wolfgang Maass, Timothée Masquelier, Richard Naud, Emre O. Neftci, Mihai A. Petrovici, Franz Scherr, and Dan F.M. Goodman. 2021. Visualizing a Joint Future of Neuroscience and Neuromorphic Engineering. *Neuron* 109, 4 (2021), 571–575.
- [58] Anguo Zhang, Jieming Shi, Junyi Wu, Yongcheng Zhou, and Wei Yu. 2023. Low Latency and Sparse Computing Spiking Neural Networks With Self-Driven Adaptive Threshold Plasticity. *IEEE Transactions on Neural Networks and Learning Systems* (2023), 1–12.
- [59] Jiqing Zhang, Bo Dong, Haiwei Zhang, Jianchuan Ding, Felix Heide, Baocai Yin, and Xin Yang. 2022. Spiking Transformers for Event-Based Single Object Tracking. In *Proceedings of the IEEE/CVF Conference on Computer Vision and Pattern Recognition*. 8801–8810.
- [60] Jiyuan Zhang, Lulu Tang, Zhaofei Yu, Jiwen Lu, and Tiejun Huang. 2022. Spike Transformer: Monocular Depth Estimation for Spiking Camera. In *European Conference on Computer Vision*. 34–52.
- [61] Wenrui Zhang and Peng Li. 2020. Temporal Spike Sequence Learning via Backpropagation for Deep Spiking Neural Networks. In *Advances in Neural Information Processing Systems*, Vol. 33. 12022–12033.
- [62] Rong Zhao, Zheyu Yang, Hao Zheng, Yujie Wu, Faqiang Liu, Zhenzhi Wu, Lukai Li, Feng Chen, Seng Song, Jun Zhu, et al. 2022. A Framework for the General Design and Computation of Hybrid Neural Networks. *Nature communications* 13, 1 (2022), 3427.
- [63] Chenlin Zhou, Liutao Yu, Zhaokun Zhou, Han Zhang, Zhengyu Ma, Huihui Zhou, and Yonghong Tian. 2023. Spikingformer: Spike-driven Residual Learning for Transformer-based Spiking Neural Network. *arXiv preprint arXiv:2304.11954* (2023).
- [64] Zhaokun Zhou, Yuesheng Zhu, Chao He, Yaowei Wang, Shuicheng YAN, Yonghong Tian, and Li Yuan. 2023. Spikformer: When Spiking Neural Network Meets Transformer. In *Proceedings of the International Conference on Learning Representations*.
- [65] Xiaolei Zhu, Baixin Zhao, De Ma, and Huajin Tang. 2022. An Efficient Learning Algorithm for Direct Training Deep Spiking Neural Networks. *IEEE Transactions on Cognitive and Developmental Systems* 14, 3 (2022), 847–856.

7 Proof of Theorem 1

THEOREM 7.1. Consider a non-linear layer l with a function F . In SNNs, the output of this layer at time t is denoted as $\mathbf{O}^l(t)$. Let $S^l(T)$ be the cumulative sum of layer l outputs up to time T , given by $S^l(T) = \sum_{t=1}^T \mathbf{O}^l(t)$. The expected output of the SNNs at time T is given by:

$$\mathbf{O}^l(T) = TF \left(\frac{S^{l-1}(T)}{T} \right) - (T-1)F \left(\frac{S^{l-1}(T-1)}{T-1} \right). \quad (31)$$

PROOF. According to Section 3.2, we denote $\mathbf{x}^l(t)$ as $\mathbf{O}^l(t)$, which has the same meaning, and we can approximate the output value of ANNs using the mean value of the output for the first T time steps in SNNs:

$$\mathbf{a}_T^l = \Phi^l(T) = \frac{\sum_{t=1}^T \mathbf{O}^l(t)}{T} \quad (32)$$

where \mathbf{a}_T^l represents the estimated values of neurons in layer l at time T in ANNs. It will change as the corresponding spikes in SNNs accumulate over time.

Meanwhile, in the case of ANNs, \mathbf{a}_T^l can be formulated as:

$$\mathbf{a}_T^l = F(\mathbf{a}_{T-1}^{l-1}). \quad (33)$$

Furthermore, we can deduce the output by subtracting the total output of the previous T and $T-1$ time steps from the formula 32 and the formula 33.

$$\begin{aligned} \mathbf{O}^l(T) &= \sum_{t=1}^T \mathbf{O}^l(t) - \sum_{t=1}^{T-1} \mathbf{O}^l(t) \\ &= T\mathbf{a}_T^l - (T-1)\mathbf{a}_{T-1}^{l-1} \\ &= TF(\mathbf{a}_{T-1}^{l-1}) - (T-1)F(\mathbf{a}_{T-1}^{l-1}) \\ &= TF \left(\frac{\sum_{t=1}^T \mathbf{O}^{l-1}(t)}{T} \right) - (T-1)F \left(\frac{\sum_{t=1}^{T-1} \mathbf{O}^{l-1}(t)}{T-1} \right) \\ &= TF \left(\frac{S^{l-1}(T)}{T} \right) - (T-1)F \left(\frac{S^{l-1}(T-1)}{T-1} \right). \end{aligned} \quad (34)$$

□

8 Proof of Theorem 2

THEOREM 8.1. Consider a module for matrix product that receives two sets of spike inputs, denoted by $\mathbf{A}_{v_a}(t)$ and $\mathbf{B}_{v_b}(t)$. These inputs are generated by neurons A and B , respectively, and are characterized by multiple thresholds v_a and v_b , as described in Section 4.3.

We can integrate the input by $\mathbf{A}(t) = \sum_{v_a} v_a \mathbf{A}_{v_a}(t)$ and $\mathbf{B}(t) = \sum_{v_b} v_b \mathbf{B}_{v_b}(t)$. Here, $\mathbf{A}(t)$ and $\mathbf{B}(t)$ are the sum matrices weighted by multiple thresholds v_a and v_b , respectively.

Let $\mathbf{S}_A(T) = \sum_{t=1}^T \mathbf{A}(t)$ and $\mathbf{S}_B(T) = \sum_{t=1}^T \mathbf{B}(t)$ represent the cumulative sum of inputs up to time T . We define $\mathbf{S}_K(T) = \mathbf{S}_A(T)\mathbf{S}_B(T)$. Then, the expected output at time T can be formulated as:

$$\mathbf{O}(T) = \frac{1}{T}\mathbf{S}_K(T) - \frac{1}{T-1}\mathbf{S}_K(T-1), \quad (35)$$

where $\mathbf{S}_K(T)$ can be calculated mainly using addition, as described by the following equation:

$$\mathbf{S}_K(T) = \mathbf{S}_K(T-1) + \mathbf{K}(T) \quad (36)$$

$$\begin{aligned} \mathbf{K}(T) &= \sum_{v_a, v_b} v_a v_b \mathbf{A}_{v_a}(T) \mathbf{B}_{v_b}(T) + \sum_{v_a} v_a \mathbf{A}_{v_a}(T) \mathbf{S}_B(T-1) \\ &\quad + \sum_{v_b} v_b \mathbf{S}_A(T-1) \mathbf{B}_{v_b}(T). \end{aligned} \quad (37)$$

PROOF. Since we approximate the value of ANNs using the mean value for the first T times in SNNs, let the expected input matrices \mathbf{A}_T , \mathbf{B}_T , and $\mathbf{O}_T = \mathbf{A}_T \mathbf{B}_T$ in ANNs be calculated based on the input spikes during the first T time steps in SNNs, denoted as:

$$\mathbf{A}_T = \frac{\sum_{t=1}^T \mathbf{A}(t)}{T} \quad (38)$$

$$\mathbf{B}_T = \frac{\sum_{t=1}^T \mathbf{B}(t)}{T} \quad (39)$$

$$\mathbf{O}_T = \frac{\sum_{t=1}^T \mathbf{O}(t)}{T} \quad (40)$$

So, the expected output matrix $\mathbf{O}(T)$ at time T can be calculated by:

$$\begin{aligned} \mathbf{O}(T) &= \sum_{t=1}^T \mathbf{O}(t) - \sum_{i=1}^{T-1} \mathbf{O}(t) \\ &= T\mathbf{O}_T - (T-1)\mathbf{O}_{T-1} \\ &= T\mathbf{A}_T \mathbf{B}_T - (T-1)\mathbf{A}_{T-1} \mathbf{B}_{T-1} \\ &= T \frac{\sum_{t=1}^T \mathbf{A}(t)}{T} \frac{\sum_{t=1}^T \mathbf{B}(t)}{T} \\ &\quad - (T-1) \frac{\sum_{t=1}^{T-1} \mathbf{A}(t)}{T-1} \frac{\sum_{t=1}^{T-1} \mathbf{B}(t)}{T-1} \\ &= \frac{1}{T} \sum_{t=1}^T \mathbf{A}(t) \sum_{t=1}^T \mathbf{B}(t) - \frac{1}{(T-1)} \sum_{t=1}^{T-1} \mathbf{A}(t) \sum_{t=1}^{T-1} \mathbf{B}(t) \\ &= \frac{1}{T} \mathbf{S}_A(T) \mathbf{S}_B(T) - \frac{1}{T-1} \mathbf{S}_A(T-1) \mathbf{S}_B(T-1) \\ &= \frac{1}{T} \mathbf{S}_K(T) - \frac{1}{T-1} \mathbf{S}_K(T-1) \end{aligned} \quad (41)$$

And $\mathbf{S}_K(T)$ can be calculated by:

$$\begin{aligned} \mathbf{S}_K(T) &= \mathbf{S}_A(T) \mathbf{S}_B(T) \\ &= (\mathbf{S}_A(T-1) + \mathbf{A}(T))(\mathbf{S}_B(T-1) + \mathbf{B}(T)) \\ &= \mathbf{S}_A(T-1) \mathbf{S}_B(T-1) + \mathbf{A}(T) \mathbf{B}(T) \\ &\quad + \mathbf{A}(T) \mathbf{S}_B(T-1) + \mathbf{S}_A(T-1) \mathbf{B}(T) \\ &= \mathbf{S}_K(T-1) + \sum_{v_a, v_b} v_a v_b \mathbf{A}_{v_a}(T) \mathbf{B}_{v_b}(T) \\ &\quad + \sum_{v_a} v_a \mathbf{A}_{v_a}(T) \mathbf{S}_B(T-1) + \sum_{v_b} v_b \mathbf{S}_A(T-1) \mathbf{B}_{v_b}(T) \\ &= \mathbf{S}_K(T-1) + \mathbf{K}(T). \end{aligned} \quad (42)$$

Assuming the dimension of $\mathbf{S}_K(T)$, $\mathbf{S}_A(T)$ and $\mathbf{S}_B(T)$ are $n \times m$, $n \times p$ and $p \times m$, respectively. And suppose the firing rate of $\mathbf{A}(T)$ and $\mathbf{B}(T)$ are η_1 and η_2 .

In order to determine the number of different operations required to update $\mathbf{S}_K(T)$, we conduct a brief analysis: Multiplications occur when the threshold is multiplied by the results of various matrix multiplications; Additions occur during the calculation of individual matrix multiplications, as well as the accumulation of the results of the four parts.

As each position of the input matrix has only one effective threshold at each time, it restricts the total number of input spikes, thus limiting the total number of operations.

The maximum addition operation number is

$$ACs_{SNN}^{max} = \eta_1 \eta_2 n p m + \eta_1 n p m + \eta_2 n p m + 3 n m \quad (43)$$

where $\eta_1 \eta_2 n p m$, $\eta_1 n p m$ and $\eta_2 n p m$ are the maximum addition operations in calculating $\sum_{v_a, v_b} v_a v_b A v_a(T) B v_b(T)$, $\sum_{v_a} v_a A v_a(T) S_B(T-1)$ and $\sum_{v_b} v_b S_A(T-1) B v_b(T)$, respectively. $3 n m$ is the maximum operation in accumulating four parts in Equation (36).

The maximum multiplication operation number is

$$MACs_{SNN}^{max} = \min(\eta_1, \eta_2) n m + \eta_1 n m + \eta_2 n m \quad (44)$$

where $\min(\eta_1, \eta_2) n m$, $\eta_1 n m$ and $\eta_2 n m$ are the maximum multiplication operations in calculating $\sum_{v_a, v_b} v_a v_b A v_a(T) B v_b(T)$, $\sum_{v_a} v_a A v_a(T) S_B(T-1)$ and $\sum_{v_b} v_b S_A(T-1) B v_b(T)$, respectively.

It can be seen that $ACs_{SNN}^{max} \gg MACs_{SNN}^{max}$, so $S_K(T)$ can be calculated mainly using addition. \square

9 Experiment Details

9.1 Datasets

CIFAR-10. The CIFAR-10 dataset [27] consists of 60000 32×32 images in 10 classes. There are 50000 training images and 10000 test images.

CIFAR-100. The CIFAR-100 dataset [27] consists of 60000 32×32 images in 100 classes. There are 50000 training images and 10000 test images.

ImageNet1k. We use the ILSVRC 2012 dataset [42], which consists of 1,281,167 training images and 50000 testing images.

9.2 Data Preprocessing

To process our image data, we followed a series of steps. First, we resized the image to the desired size and then cropped it to match the input size. After that, we converted the image into a PyTorch tensor. Next, we normalized the pixel values using the provided mean and standard deviation values. The mean and standard deviation values were specified as (0.48145466, 0.4578275, 0.40821073) and (0.26862954, 0.26130258, 0.27577711). Finally, we normalized the pixel values of the three-channel images based on the provided mean and standard deviation.

9.3 Experimental Setup

The conversion in this paper is based on pre-trained Vision Transformer including the ViT-S/16, ViT-B/16, ViT-L/16 with 224 resolution [47], and the EVA model `eva_g_patch14` in [17].

For all Multi-Threshold Neurons, we set n to 8 for ViT-S/16, ViT-B/16, ViT-L/16 and 6 for EVA. We set threshold percent p to 99 to get thresholds for each neuron. In particular, due to huge differences in GELU and softmax layers' output values, we configure the positive and negative base thresholds to 0.5 and 0.08, respectively, for neurons following the GELU module in ViT models, and to

0.0125 for neurons following the softmax module to prevent too few spikes.

Besides, the precision of the network is highly sensitive to the precision of the classification layer, as mentioned in [29]. Since the classification layer has minimal energy consumption during runtime, we retained analog input in the classification layer.

10 Additional Experimental Details

10.1 Detailed results on other datasets

Tables 4 and 5 present a comparison of the accuracy and energy consumption of different neural network architectures - ANNs and SNNs - on CIFAR10 and CIFAR100 datasets.

Table 4 compares the accuracy of ANN and SNN architectures for the CIFAR10 dataset across three model scales: ViT-S/16, ViT-B/16, and ViT-L/16. It can be seen that the SNN model can reach a comparable accuracy while significantly reducing the consumption. For example, when the SNN model is run for 6 time steps, models such as ViT-S/16, ViT-B/16, and ViT-L/16 achieve accuracy levels of 97.37%, 98.24%, and 99.1%, respectively. The remarkable fact is that they only consume 0.6, 0.48, and 0.4 energy, respectively when compared to the original ANN (Artificial Neural Network) models.

Table 5 presents a similar comparison for the more complex CIFAR100 dataset. For instance, at 6 timesteps, ViT-S/16, ViT-B/16, and ViT-L/16 achieve accuracies of 84.75%, 90.22%, and 93.04%, respectively, while using only 0.61, 0.48, and 0.43 energy compared to original ANN models. It shows the potential of our method to reduce energy consumption while maintaining accuracy. The results demonstrate our method's potential to reduce energy consumption while maintaining accuracy.

10.2 Comparison with the State-of-the-art on CIFAR10 and CIFAR100 datasets

We compare the experimental results using the ViT-S/16, ViT-B/16, ViT-L/16 model on the CIFAR10 and CIFAR100 datasets with previous state-of-the-art methods, as shown in Table 6 and 7.

In the evaluation of the CIFAR10 dataset, the ECMT model achieved an impressive accuracy rate of 97.37%, 98.24%, and 99.1% respectively, using the architecture of ViT-S/16, ViT-B/16, ViT-L/16 over just six timesteps. This level of precision is highly competitive, especially compared to similarly-sized models. In evaluating the CIFAR100 dataset, considered more complex, the ECMT method again displays its strength. The results demonstrate that the ECMT method achieves a similar high accuracy.

The ECMT model uses the Transformer-to-SNN approach and has performed exceptionally well on the CIFAR10 and CIFAR100 datasets. Its ViT-B/16 variant stands out by achieving high accuracy with a moderate number of parameters, indicating the potential of SNNs in achieving state-of-the-art results with a significant reduction in computational resources. This balance of efficiency and accuracy makes the ECMT a promising model for energy-efficient and fast processing tasks.

Table 4: Accuracy and energy consumption ratio of ECMT(Ours) on CIFAR10 dataset

Arch.	Accuracy/Energy	Original (ANN)	Ours (SNN)					
			T=1	T=2	T=4	T=6	T=8	T=10
ViT-S/16	Acc. (%)	98.33	8.53	31.32	93.82	97.37	98.01	98.21
	Energy ratio	1	0.06	0.15	0.37	0.60	0.82	1.03
ViT-B/16	Acc. (%)	98.75	9.17	32.25	95.17	98.24	98.55	98.69
	Energy ratio	1	0.04	0.12	0.30	0.48	0.66	0.83
ViT-L/16	Acc. (%)	99.07	10.55	95.14	98.89	99.1	99.03	99.08
	Energy ratio	1	0.03	0.11	0.27	0.42	0.57	0.72

Table 5: Accuracy and energy consumption ratio of ECMT(Ours) on CIFAR100 dataset

Arch.	Accuracy/Energy	Original (ANN)	Ours (SNN)					
			T=1	T=2	T=4	T=6	T=8	T=10
ViT-S/16	Acc. (%)	89.28	0.95	4.9	69.49	84.75	87.83	88.93
	Energy ratio	1	0.06	0.16	0.38	0.61	0.84	1.07
ViT-B/16	Acc. (%)	92.26	0.87	17.07	82.86	90.22	91.5	91.91
	Energy ratio	1	0.04	0.12	0.30	0.48	0.66	0.84
ViT-L/16	Acc. (%)	93.84	1.61	69.08	91.82	93.04	93.34	93.56
	Energy ratio	1	0.04	0.12	0.27	0.43	0.58	0.73

Table 6: Comparison between the proposed method and previous works on CIFAR10 dataset

Method	Type	Arch.	Param. (M)	T	Accuracy (%)
Spikingformer[63]	Direct Training	Spikingformer-4-384-400E	9.32	4	95.81
Spike-driven Transformer[55]	Direct Training	Spikingformer-4-384-400E	9.32	4	95.6
RMP[19]	CNN-to-SNN	VGG-16	138	64(2048)	90.35(93.63)
SNM[50]	CNN-to-SNN	VGG-16	138	32(128)	93.43(94.07)
TS[9]	CNN-to-SNN	VGG-16	138	16(32)	92.29(92.29)
QFFS[29]	CNN-to-SNN	VGG-16	138	4	92.64
QCFS[3]	CNN-to-SNN	ResNet-18	11.8	8(64)	94.82(96.06)
		VGG-16	138	8(64)	94.95(95.55)
SRP[21]	CNN-to-SNN	ResNet-18	11.8	4(16)	95.25(95.55)
		VGG-16	138	4(16)	95.32(95.42)
MST[51]	Transformer-to-SNN	Swin-T(BN)	27.6	64(256)	96.32(97.27)
STA[26]	Transformer-to-SNN	ViT-B/32	86	32(256)	95.49(95.82)
ECMT(Ours)	Transformer-to-SNN	ViT-S/16	22	6(8)	97.37(98.01)
		ViT-B/16	86	6(8)	98.24(98.55)
		ViT-L/16	307	6(8)	99.1(99.03)

Table 7: Comparison between the proposed method and previous works on CIFAR100 dataset

Method	Type	Arch.	Param. (M)	T	Accuracy (%)
Spikingformer[63]	Direct Training	Spikingformer-4-384-400E	9.32	4	79.21
Spike-driven Transformer[55]	Direct Training	Spikingformer-4-384-400E	9.32	4	78.4
RMP[19]	CNN-to-SNN	VGG-16	138	128(2048)	63.76(70.93)
SNM[50]	CNN-to-SNN	VGG-16	138	32(128)	71.8(73.95)
TS[9]	CNN-to-SNN	VGG-16	138	16(64)	63.73(69.27)
QCFS[3]	CNN-to-SNN	ResNet-18	11.8	8(64)	78.48(79.54)
		VGG-16	138	8(64)	73.96(77.10)
SRP[21]	CNN-to-SNN	ResNet-20	0.27	4(32)	59.34(65.50)
		VGG-16	138	4(32)	75.42(76.45)
MST[51]	Transformer-to-SNN	Swin-T(BN)	27.6	64(256)	85.4(86.91)
STA[26]	Transformer-to-SNN	ViT-B/32	86	32(256)	84.15(85.98)
ECMT(Ours)	Transformer-to-SNN	ViT-S/16	22	6(8)	84.75(87.83)
		ViT-B/16	86	6(8)	90.22(91.5)
		ViT-L/16	307	6(8)	93.04(93.34)